

## Analytical transmission electron microscopy study of a natural MORB sample assemblage transformed at high pressure and high temperature

ANGÈLE RICOLLEAU,<sup>1,\*</sup> GUILLAUME FIQUET,<sup>1</sup> AHMED ADDAD<sup>2</sup>, NICOLAS MENGUY,<sup>1</sup>  
CHRISTIAN VANNI,<sup>3</sup> JEAN-PHILIPPE PERRILLAT,<sup>4</sup> ISABELLE DANIEL,<sup>4</sup> HERVÉ CARDON,<sup>4</sup>  
AND NICOLAS GUIGNOT<sup>5</sup>

<sup>1</sup>Institut de Minéralogie et de Physique des Milieux Condensés, UMR7590, Université Paris VI et VII, Institut de Physique du Globe de Paris, 140 Rue de Lourmel, F-75015, France

<sup>2</sup>Laboratoire de Structure et Propriétés de l'Etat Solide, ESA CNRS 8008-Bâtiment C6, Université des Sciences et Technologie de Lille, 59655 Villeneuve d'Ascq Cedex, France

<sup>3</sup>Laboratoire CP2M Faculté des Sciences et Techniques de Saint Jérôme, Université d'Aix-Marseille, III, F-13397 Marseille Cedex 20, France

<sup>4</sup>Laboratoire de Sciences de la Terre, UMR5570, CNRS-UCB Lyon1-ENS Lyon, Bat. Géode, 2 Rue Raphaël Dubois, F-69622 Villeurbanne Cedex, France

<sup>5</sup>European Synchrotron Radiation Facility, BP220, F-38043 Grenoble, France

### ABSTRACT

Natural mid-ocean ridge basalt (MORB) samples recovered from diamond-anvil cell (DAC) experiments performed between 33 to 89 GPa and 1700 to 2600 K were studied with a transmission electron microscope (TEM). We used the focused ion beam (FIB) lift-out technique to prepare the recovered high-pressure, laser-heated samples for TEM study. Observations of TEM sections show the presence of five phases for samples transformed at pressures ranging from 33 to 45 GPa: Al-bearing Mg-perovskite, Ca-silicate perovskite, stishovite, and two Al-rich phases. The Al-rich phases were identified by selected area electron diffraction (SAED) patterns and chemical composition analysis, and include the new aluminous (NAL) phase with hexagonal structure and the calcium ferrite (CF) type phase. Chemical analyses obtained by analytical transmission electron microscopy (ATEM) show that Mg-silicate perovskite is the major host for Al, with significant amounts also distributed between the CF-type and NAL phases, and less than 1 wt% in stishovite. Beyond pressures of ~40 GPa (~1100 km depth), the Al content of Mg-perovskite and CF-type phase increases. Between 45 and 50 GPa, the NAL phase disappears. This mineralogical change may explain reported seismic anomalies in subduction zones at mid-mantle depths.

**Keywords:** High-pressure phases, ATEM, aluminous phases, high-pressure MORB samples, lower mantle, perovskite

### INTRODUCTION

The fate of subducted oceanic crust in the deep Earth has been the subject of numerous investigations (e.g., Kesson et al. 1994; Ono et al. 2005). Such studies require a detailed knowledge of the phases involved and their respective chemical compositions. With the exception of a few pioneering studies at pressures exceeding 40 GPa involving diamond-anvil cell experiments, X-ray diffraction (XRD), and/or transmission electron microscope (TEM) on MORB and peridotite compositions (Funamori et al. 2000; Lee et al. 2004a, 2004b; Hirose et al. 2005; Murakami et al. 2005; Ono et al. 2005), most petrological studies have been performed using multi-anvil apparatuses at transition-zone conditions, up to 37 GPa (Ono et al. 2001). These experimental studies on MORB compositions at transition-zone conditions have reported up to five phases (Irifune and Ringwood 1993; Hirose et al. 1999; Litasov et al. 2004): Al-bearing Mg-perovskite,

Ca-perovskite, stishovite, and two aluminous phases, i.e., the calcium ferrite (CF) type phase, and the new aluminous (NAL) phase. Miyajima et al. (1999, 2001) reported the presence of the NAL phase after re-examination of experiments from Irifune and Ringwood (1993) and Hirose et al. (1999); however, other studies performed on MORB at pressures up to 130 GPa have reported only one Al-rich phase (CF) in their assemblage (Kesson et al. 1994; Funamori et al. 2000; Hirose et al. 2005).

Liu (1977) initially proposed the CF-type phase as a potential host mineral for Al and Na with an NaAlSiO<sub>4</sub> end-member composition. CF was first described in high-pressure MORB by Irifune and Ringwood (1993). Subsequently, the thermodynamic properties of the MgAl<sub>2</sub>O<sub>4</sub> and NaAlSiO<sub>4</sub> end-members as well as MORB relevant compositions were studied up to 70 GPa (Yutani et al. 1997; Funamori et al. 1998; Tutti et al. 2000; Dubrovinsky et al. 2002; Ono et al. 2002a; Guignot and Andraut 2004). Funamori et al. (1998) observed that, above 40 GPa, the MgAl<sub>2</sub>O<sub>4</sub> end-member undergoes a transformation from the CaFe<sub>2</sub>O<sub>4</sub>-like structure into a CaTi<sub>2</sub>O<sub>4</sub>-like structure. The CaTi<sub>2</sub>O<sub>4</sub> structure was also reported by Ono et al. (2005) at 143 GPa in a MORB composition.

\* Present address: Geophysical Laboratory, Carnegie Institution of Washington, 5251 Broad Branch Road, Washington, D.C. 20015, U.S.A. E-mail: a.ricolleau@gl.ciw.edu

The NAL phase is an important phase in natural MORB samples and is one of the stable phases formed when garnet decomposes (Miyajima et al. 1999, 2001; Oguri et al. 2000). Various studies have provided information about the structure, stability, and equation of state of the NAL phase (e.g., Gasparick et al. 2000; Miura et al. 2000; Guignot and Andraut 2004; Shinmei et al. 2005). It appears that the NAL phase is stable up to at least 63 GPa (Ono et al. 2002b). Guignot and Andraut (2004) found significant changes in the bulk modulus of the NAL phase as a function of composition; however, the study of Vanpeteghem et al. (2003) did not confirm this observation.

Although multi-anvil experiments (e.g., Hirose et al. 1999; Litasov et al. 2004) and DAC experiments (e.g., Kesson et al. 1994; Funamori et al. 2000; Hirose et al. 2005; Ono et al. 2005) both confirm the presence of Al-bearing Mg-perovskite, Ca-perovskite, and stishovite phases up to 130 GPa in MORB, only multi-anvil studies have reported the coexistence of two aluminous phases. DAC experiments at lower-mantle pressures find only the CF-type phase. The coexistence of NAL and CF phases reported in multi-anvil experiments was recently questioned by Sanehira et al. (2006). These authors proposed that only the NAL phase is stable at high-pressure–high-temperature conditions, and that it partly transforms to the CF-type phase during quenching. The nature and the stability field of the Al-phases with respect to  $P/T$  conditions are therefore still uncertain.

In this paper, we report the behavior of MORBs at high-pressure and temperature on the basis of high-resolution TEM observations. We present a TEM study on MORB samples recovered after high-pressure–high-temperature in situ XRD experiments carried out between 33 and 89 GPa and from 1700 to 2600 K (Ricolleau et al. 2004; Perrillat et al. 2006). We show that the focused ion beam (FIB) technique is particularly well-suited to prepare samples recovered from high-pressure experiments in diamond-anvil cells for TEM observations. We report the mineralogical and chemical compositions of run products at various pressures, confirm the coexistence of the NAL and the CF-type phases as host phases for Al and Na, and map their  $P/T$  stability fields. We confirm the disappearance of the NAL phase during in situ XRD measurements at pressures exceeding 50 GPa (Perrillat et al. 2006). Finally, we discuss the chemical evolution of the high-pressure phases in relation to mineralogical changes and the possible implications for seismic observations in mantle subduction zones.

## EXPERIMENTAL TECHNIQUES

### Sample synthesis and preparation for TEM investigations by FIB

Natural MORB pillow glass from the East-Pacific Rise (see composition in Table 1) was loaded in neon using rhenium gaskets, in Chervin-type DAC (Chervin et al. 1995). Type IA diamonds with flat culets of 300  $\mu\text{m}$  or beveled diamonds with 300–150  $\mu\text{m}$  culets were used. Neon was used as the pressure-transmitting medium, except for MORB8 at 89 GPa that was loaded without a pressure medium. A single ruby sphere was placed close to the sample to measure the pressure by ruby fluorescence before laser heating (Mao et al. 1986). During laser heating, pressures cannot be estimated from the ruby fluorescence scale or the equation of state (EoS) of the transmitting pressure medium because of the high thermal gradient between the sample and the pressure medium. Consequently, pressures were determined using the diffraction lines of stishovite grains, which crystallized in the sample, with the thermal EoS of Liu et al. (1999). At 300 K, pressures mea-

sured from the EoS of stishovite were in good agreement ( $\pm 1$  GPa or 2–3%) with pressures obtained from the EoS of neon (Hemley et al. 1989). Finally, studies on MORB composition by Ono et al. (2005) and Hirose et al. (2005), using gold as a pressure calibrant at high temperature, yielded pressures agreeing within 4% with those calculated with stishovite. Stishovite therefore appears to provide a reliable internal pressure scale using the EoS from Liu et al. (1999). Transformation of stishovite from the rutile-type to the  $\text{CaCl}_2$ -type structure has been reported around 55 GPa (e.g., Andraut et al. 1998; Oganov et al. 2005). We observed the  $\text{CaCl}_2$ -type structure in XRD spectra obtained at 89 GPa on MORB8. This transformation had not been observed at 55 GPa and high temperature, i.e., MORB5, as reported by Perrillat et al. (2006).

Samples were first pressurized at ambient temperature to 26 GPa for MORB1, 36 GPa for MORB4, 43 GPa for MORB5, and 78 GPa for MORB8, and then laser heated in the temperature range 1700–2600 K using the double-sided laser-heating system developed around two TEM<sub>00</sub> Nd:YAG lasers (40W each) available at the ID 30 (now ID 27) beamline at the European Synchrotron Radiation Facility (ESRF) in Grenoble, France (see Schultz et al. 2005 for optical details). The laser-heated spot is typically 30  $\mu\text{m}$  in diameter. The transformation of the glass starting material to the high-pressure phase assemblage at a given pressure was systematically achieved by heating the sample over at least 10 min at temperatures around 2000 K. The pressure generally increases 3 to 10 GPa during heating (Fig. 1). Each heating condition was maintained stable for more than 10 min in a  $\pm 150$  K range while an XRD spectrum was recorded (see Perrillat et al. 2006 for experimental details). Spectra were acquired every 100–200 K such that the entire experiment took several hours. The laser beam was kept at the same position for one entire heating cycle to avoid temperature gradients and possible resulting chemical gradients that would be created by scanning across the sample. Once spectra were obtained at the highest temperatures of interest, the samples were quenched by shutting off infrared lasers. For sample MORB8, the pressure was subsequently increased to 85 GPa for the acquisition of another high-temperature data set. The pressure-temperature conditions are summarized in Figure 1.

Quenched samples are approximately  $60 \times 60 \mu\text{m}^2$  in size (Fig. 2a), which makes the traditional Ar ion milling preparation nearly impossible—we therefore used the focused ion beam technique (FIB). Although the FIB was initially developed for semiconductor studies (Giannuzzi and Stevie 1999), it is now widely used for geological samples like minerals (Heaney et al. 2001; Reusser et al. 2003) or for geomicrobiology applications (Benzerara et al. 2005). Recently, the FIB technique was successfully used on DAC samples (Irifune et al. 2005). FIB is a site-specific technique for the preparation of TEM thin sections and requires minimum sample manipulation. The recovered samples can be directly placed on a conducting carbon tape attached to a classical SEM sample holder for further FIB preparation. FIB milling was performed using a FEI Model 200 TEM FIB system at the University Aix-Marseille III. We used the FIB “lift-out” technique described in detail by Giannuzzi and Stevie (1999). A thin layer of platinum was deposited on

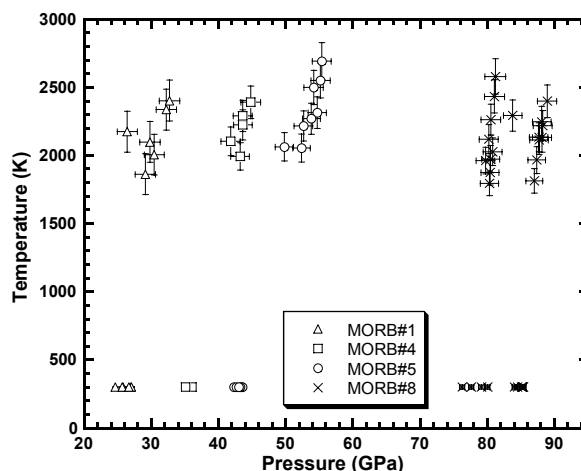
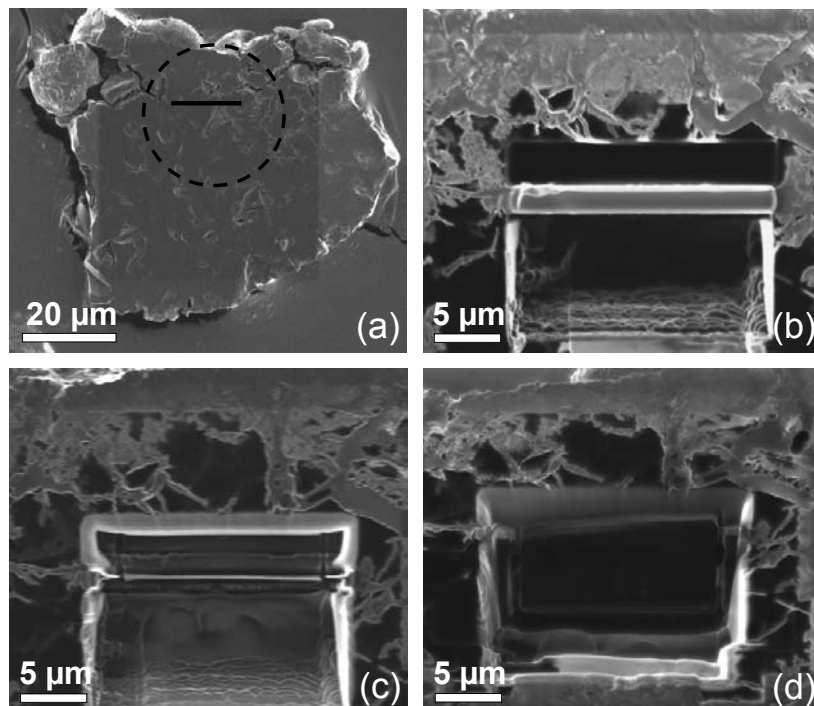
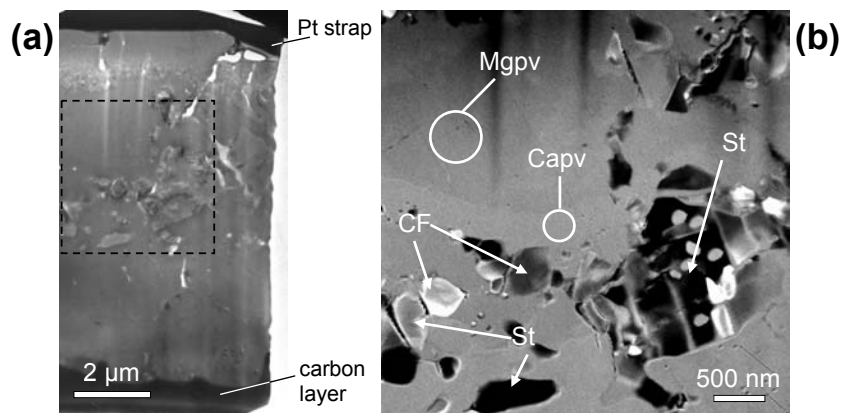


FIGURE 1. Pressure-temperature measurements after complete transformation of the starting glass material. Triangles correspond to sample MORB1, squares to sample MORB4, circles to sample MORB5, and crosses to sample MORB8.



**FIGURE 2.** (a) Image of a quenched sample transformed at 50–55 GPa obtained under a flux of  $\text{Ga}^+$  ions. The sample is placed on carbon tape and coated with carbon to avoid electrical charge build-up at the sample surface during focused ion beam (FIB) operation. The sample is around  $65 \times 55 \mu\text{m}$ . The dotted circle represents the laser heated spot, and the back line indicates the site of the FIB thin section. Stages of sample extraction: (b) picture of the cross-section zone after sputtering the staircase in front of the platinum strap and the hole behind it; (c) at the end of the sputtering: the 100 nm thick cross-section that will be removed from the matrix; (d) same image with a tilt of  $45^\circ$ . The cross-section is 15  $\mu\text{m}$  in length and 10  $\mu\text{m}$  in width.



**FIGURE 3.** Transmission electron microscopy (TEM) bright-field micrograph of the FIB cross-section. (a) This picture shows a part of the FIB thin section extracted from the laser heated spot shown in Figure 2. Along the vertical direction, this represents a whole cross-section of the sample, delimited by the platinum strap on one side and the conducting carbon layer on the other side. This direction also corresponds to the axial temperature gradient (optical axis of the DAC) created by infrared lasers. This gradient, however, is thought to be limited with a measured sample thickness of only 8.5  $\mu\text{m}$ . (b) Scanning TEM image showing sample microstructure. Grains of stishovite (St) and calcium ferrite-type phase (CF) are surrounded by a matrix of amorphous Mg-perovskite (Mgpv) and Ca-perovskite (Capv).

top of the region of interest to prevent surface degradation. The FIB system uses a Ga liquid metal ion source that allows milling. A 30 kV  $\text{Ga}^+$  beam operating at  $\sim 20$  nA excavated the sample from both sides of the Pt layer to a depth of  $\sim 5 \mu\text{m}$ , allowing us to obtain a thin cross-section (Fig. 2b). Before removal of the cross-section, the sample was further thinned to  $\sim 100$  nm with a beam operating at  $\sim 100$  pA current and sample tilt of  $1.2^\circ$  (Fig. 2c). Finally, a line pattern was drawn with the ion beam along the side and bottom edges of the cross-section, allowing its removal (Fig. 2d).

The final section (size of  $\sim 15 \mu\text{m} \times \sim 5 \mu\text{m} \times \sim 100$  nm) was then deposited onto a membrane of carbon-coated 200-mesh copper grid using a stereomicroscope and a hydraulic micromanipulator. The cross-sections display variable thickness (50 nm to 350 nm) due to the path of  $\text{Ga}^+$  ions and the variable hardness of phases in our samples. A typical TEM picture of one section is shown in Figure 3. In this example, we cut through the whole sample and obtained a cross-section of 10  $\mu\text{m}$  length, in which the high pressure recovered sample is about 8.5  $\mu\text{m}$  thick (Fig. 3a).

**TABLE 1.** Chemical composition of high-pressure phases in a MORB starting composition

Pressure	This study			A	B			C	D	E	
	MORB1 33 GPa	MORB4 44 GPa	MORB5 55 GPa	27 GPa	30 GPa	33 GPa	37 GPa	45 GPa	43.2GPa	60 GPa	
wt%	<b>SM</b>										
wt%	<b>Mgpv</b>										
SiO <sub>2</sub>	49.74 (0.49)	45.4 (1.9)	42.3 (1.4)	40.9 (0.6)	37.38	34.7	32.4	37.5	40.6	43.2	41.5 (2.4)
TiO <sub>2</sub>	1.33 (0.13)	3.6 (0.0)	2.5 (0.3)	2.1 (0.2)	3.58	4.7	4.3	4.5	2.1	1.3	2.4 (0.5)
Al <sub>2</sub> O <sub>3</sub>	15.89 (0.23)	13.4 (0.7)	21.2 (1.4)	23.6 (0.9)	16.14	15.1	19.2	13	16.4	22.1	13.7 (1.9)
FeO	9.73 (0.28)	14.0 (0.9)	11.3 (1.4)	10.1 (0.5)	23.01	20.9	20.1	20.6	17	12.7	20.1 (1.2)
MgO	8.46 (0.12)	20.8 (2.0)	18.7 (1.2)	19.1 (0.6)	17.85	21.1	19	21.3	22.6	17.2	21.3 (3.2)
CaO	11.74 (0.19)	2.7 (1.5)	3.5 (0.7)	3.3 (0.3)	1.65	0.3	0.5	0.8	0	2.2	1.0 (0.6)
Na <sub>2</sub> O	2.69 (0.09)	0.0 (0.0)	0.5 (0.3)	0.8 (0.2)	0.87	0.3	0.5	0.6	0.8	1.4	–
Prop (wt%)	23 (5)	38 (5)	40 (4)								
wt%	<b>St</b>										
SiO <sub>2</sub>	98.8 (0.3)	98.7 (0.4)	98.5 (0.4)	96.82	93.9	95.5	96.9	96.5	96.3	96.6 (1.1)	
TiO <sub>2</sub>	0.1 (0.1)	0.1 (0.1)	0.1 (0.1)	0.11	0	0.1	0	0	–	–	
Al <sub>2</sub> O <sub>3</sub>	0.5 (0.2)	0.8 (0.2)	0.9 (0.1)	1.26	4.2	3.7	2.6	2.8	2.5	3.4 (1.1)	
FeO	0.1 (0.2)	0.1 (0.1)	0.1 (0.1)	0.46	0.3	0.2	0.2	0	0.2	–	
MgO	0.0 (0.1)	0.0 (0.1)	0.1 (0.1)	0.38	0	0.2	0	0	0.4	–	
CaO	0.4 (0.3)	0.1 (0.1)	0.4 (0.3)	0.36	0	0.1	0.1	0	0.3	–	
Na <sub>2</sub> O	0.0 (0.0)	0.0 (0.0)	0.0 (0.0)	0.16	0	0	0.1	0	0.3	–	
Prop (wt%)	17 (2)	15 (2)	16 (1)								
wt%	<b>Capv</b>										
SiO <sub>2</sub>	51.6 (0.1)	51.9 (0.4)	52.1 (0.2)	43.2	46.6	46	48	56.5	51.0	50.3 (2.1)	
TiO <sub>2</sub>	1.3 (0.4)	1.3 (0.2)	1.2 (0.1)	1.56	2.3	1.5	0.9	0	0.9	0.3 (0.2)	
Al <sub>2</sub> O <sub>3</sub>	3.3 (0.4)	3.5 (0.8)	2.5 (0.7)	4.49	1.5	1.9	1.2	2.3	6.8	2.9 (0.6)	
FeO	3.5 (1.3)	4.4 (0.9)	3.5 (0.6)	3.45	0.4	0.9	0.7	0.8	5.9	0.8 (0.6)	
MgO	1.4 (1.1)	3.2 (1.5)	3.9 (1.1)	0.89	0.3	0.7	0.2	0.5	2.8	1.6 (0.4)	
CaO	38.8 (2.5)	35.7 (1.8)	36.8 (2.5)	39.5	44.5	43.4	41.7	39.9	30.7	42.9 (0.9)	
Na <sub>2</sub> O	0.0 (0.0)	0.1 (0.1)	0.1 (0.1)	0.68	0.6	0.6	0.8	0	2.0	0.8 (0.4)	
Prop (wt%)	28 (2)	30 (2)	29 (2)								
wt%	<b>CF</b>										
SiO <sub>2</sub>	26.0 (1.3)	28.5 (2.1)	26.7 (0.4)	26.96	27.5	27.9	28.9	23.6	27.7	28.7 (2.6)	
TiO <sub>2</sub>	0.4 (0.2)	0.5 (0.3)	0.2 (0.1)	0.92	0.7	0.7	0.7	0	0.4	1.6 (0.7)	
Al <sub>2</sub> O <sub>3</sub>	37.8 (0.9)	39.8 (1.9)	43.2 (1.3)	32.78	40.1	37.6	36.6	45.1	39.3	35.5 (2.9)	
FeO	14.0 (0.5)	9.7 (2.4)	6.2 (1.1)	16.19	7.9	7.1	6.7	7.8	7.1	10.5 (2.8)	
MgO	12.7 (1.7)	11.0 (3.3)	12.9 (1.7)	10.74	10	10	7.1	11.7	10.8	9.0 (2.6)	
CaO	1.3 (0.3)	1.3 (0.4)	1.7 (0.6)	1.87	0.8	1.3	0.5	0.9	2.3	2.2 (2.3)	
Na <sub>2</sub> O	7.9 (1.5)	9.2 (1.1)	9.1 (0.2)	11.15	12.1	13.2	15.2	10.7	12.5	12.5 (1.2)	
Prop (wt%)	22 (5)	12 (3)	15 (2)								
wt%	<b>NAL</b>										
SiO <sub>2</sub>	26.5 (1.5)	23.3 (0.4)		23.6							
TiO <sub>2</sub>	0.3 (0.2)	0.3 (0.1)		1.1							
Al <sub>2</sub> O <sub>3</sub>	38.9 (2.2)	45.0 (0.7)		37.9							
FeO	8.7 (1.0)	4.7 (0.4)		16.3							
MgO	17.7 (1.2)	18.9 (0.6)		12.3							
CaO	2.2 (0.4)	1.9 (0.4)		1.3							
Na <sub>2</sub> O	5.9 (0.4)	5.9 (0.2)		6.2							
Prop (wt%)	10 (5)	6 (2)									

Notes: SM = The composition of the starting material was determined using electron microprobe (Perrillat et al. 2006) and also contains 0.10 (0.04) wt% K<sub>2</sub>O. Mgpv = Al-bearing magnesium perovskite; St = stishovite; Capv = calcium perovskite; CF = calcium ferrite-type phase; NAL = new aluminous phase. Phase proportions were obtained by mass balance assuming that the measured chemical composition of each phase times its modal proportion must equal the bulk chemical composition of the starting material. Numbers in parenthesis indicate the standard deviation (1σ). A values correspond to analysis performed by Hirose et al. (1999) and Miyajima et al. (2001) for NAL; B values were obtained by Ono et al. (2001); C by Kesson et al. (1994); D by Funamori et al. (2000); and E by Hirose et al. (2005).

## Mineral identification by TEM

Selected area electron diffraction (SAED) patterns of product phases were obtained on a 200 kV JEOL-2100F transmission electron microscope at the Institut de Minéralogie et de Physique des Milieux Condensés (Paris, France). For the large grains (>200 nm), we obtained a minimum of two SAED patterns, which allowed us to accurately identify the high-pressure phases that were present. Figure 3b shows the microstructure of a high-pressure sample with the phases identified by SAED.

## ATEM investigations

The chemical composition of the recovered samples was measured at Laboratoire de Structure et Propriétés de l'Etat Solide in Lille (France) with a Phillips CM30 transmission electron microscope operating at 300 kV and equipped with a NORAN energy dispersive X-ray (EDX) spectrometer. This EDX is equipped with a Ge detector and an ultrathin window, which allows the detection and quantification of oxygen. The K factors (Cliff and Lorimer 1975) were determined experimentally for all elements of interest, following the method of Van Cappellen (1990). For the absorption correction, we used a method developed by Van Cappellen and Doukhan (1994), in which the thickness parameter is adjusted in the quantification program until the resultant composition fits the electroneutrality condition, i.e., the oxygen atomic concentration is equal to the sum of the atomic concentrations of the

cations multiplied by their respective valencies. EDX analyses were made in TEM scanning mode with a window of 50 × 50 nm to avoid amorphization of mineral grains and to prevent loss of alkalis. When grains were too small, the probe size was reduced to about 10 nm. Since irradiation causes some elements to migrate outside of the analyzed volume, we recorded the concentration of elements as a function of irradiation duration for each analysis (an example is shown in Fig. 4 for a CF-type phase). Our observations reveal that these effects are significant for the quantification of Na and Ca, and moderate for Al and Mg. It also appears that these effects are phase dependent, i.e., the loss of Ca in the amorphous Ca-perovskite is more important (around 10%) than in a crystallized phase, such as the CF-type phase. Similar observations were reported by Carrez et al. (2001) for Mg in olivine. Thus, compositions in atom% were extrapolated at  $t = 0$  s using an exponential law (see Carrez et al. 2001). Despite these measures, the Ca-perovskite remained slightly non-stoichiometric with high Si and low Ca contents. Due to the large effect of irradiation on this phase, we had to correct the Ca content of Ca-perovskite by approximately 20% to obtain the expected stoichiometry.

With FIB preparation, it is impossible to prevent the introduction of Ga atoms into the FIB thin section. Since the GaL $\alpha$  line is very close to the NaK $\alpha$  line, the EDX software does not resolve these two peaks. The situation is exacerbated by the high concentration of Ga relative to Na, such that the Na peak is often masked by a large Ga peak. The Na content is therefore underestimated in CF and NAL

by almost a factor of two. The Na contents of the CF and NAL phases that we report in Table 1 have been corrected so as to obtain the expected stoichiometry. Additional measurements were carried out by electron energy-loss spectroscopy (EELS) on the 200 kV JEOL-2100F TEM equipped with a Gatan GIF system to cross-check the Al content in stishovite.

## RESULTS

### Description of phases

Cross-sections were obtained on each sample recovered from 26–33, 42–45, 50–55, and 87–89 GPa. Bright-field observations of TEM thin sections and SAED patterns revealed the presence of five phases in the two lower-pressure samples (MORB1 and MORB4): stishovite, Al-bearing Mg-perovskite, Ca-perovskite, and two Al-rich phases (new Al phase NAL, and calcium ferrite CF-type phase). The same assemblage, with the exception of the NAL phase, was observed in samples synthesized at 55 and 89 GPa (MORB5 and MORB8). These results are in good agreement with our corresponding in situ XRD study (Ricolleau et al. 2004; Perrillat et al. 2006).

Stishovite was identified in all samples; an example is shown in Figure 5 for the sample recovered from 55 GPa. The two perovskite structures (Al-bearing Mg-perovskite and Ca-perovskite) are also present in all samples. Although the two

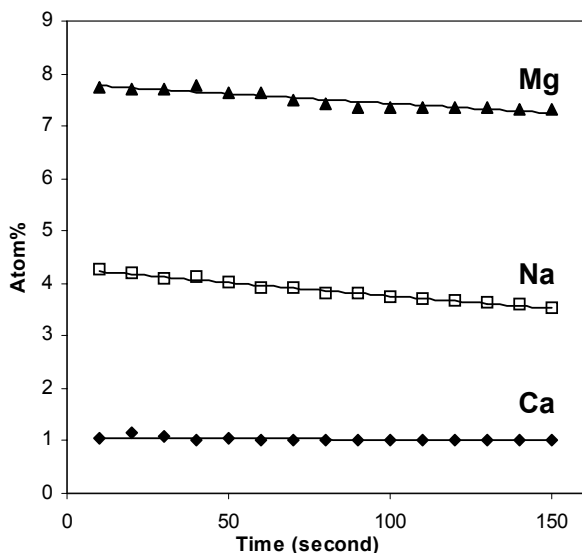


FIGURE 4. Composition in atom% of principal elements that migrated because of irradiation obtained as a function of time during analysis of a CF-type phase.

perovskites are amorphous in our TEM observations, perovskite structures were identified in the in-situ XRD data (Ricolleau et al. 2004; Perrillat et al. 2006). In addition to their respective compositional differences, the two perovskite phases are easily distinguished by their difference in contrast as observed in TEM images (Fig. 6).  $\text{CaSiO}_3$  perovskite is known to be unquenchable and to amorphize at ambient pressure (e.g., Ringwood and Major 1971). The Al-bearing Mg-perovskite is also amorphous in our cross-sections. Rapid amorphization under an electron beam is characteristic for this high-pressure metastable phase (e.g., Madon et al. 1989). We suspect that the FIB sample preparation is also likely to amorphize this phase. Aluminum-bearing Mg-perovskite is also reportedly unquenchable (Andraut et al. 2001; Yagi et al. 2004). We confirm the observations of Funamori et al. (2000) who noticed the amorphization of Al-bearing Mg-perovskite with small quantities of residual perovskite structure in their in situ XRD patterns once the assemblage is quenched to ambient conditions, as shown in Figure 7. There is indeed a clear difference between X-ray spectra obtained at 43 GPa and those collected at ambient pressure. At ambient pressure, the Ca-perovskite reflections have completely vanished and the Mg-perovskite peaks are much less intense. The extent of amorphization can be grossly estimated from the proportions of crystalline phases during decompression. The ratio of Mg-perovskite to stishovite obtained by Rietveld refinement using the GSAS package (Larson and Von Dreele 1994) is around 3 at 43 and 30 GPa, and 0.7 at ambient pressures, whereas the ratio between the CF-type phase and stishovite remains around 0.65. These findings indicate that a minimum of 70 to 80% of the Al-bearing Mg-perovskite amorphized during decompression.

Two phases containing Na and a large amount of Al are present at 33 and 44 GPa. These phases were identified by their SAED patterns as the NAL phase and the CF-type phase, previously observed in TEM studies of high-pressure MORB compositions (e.g., Funamori et al. 2000; Miyajima et al. 2001). Analysis of several SAED patterns is in good agreement with the hexagonal NAL phase structure proposed by Gasparick et al. (2000) and Miura et al. (2000) (Fig. 8). In samples synthesized at 55 and 89 GPa, we are left with only one Al-bearing phase having the calcium ferrite structure reported by Yamada et al. (1983) (Fig. 9).

### Chemical composition of phases

Chemical compositions of product phases were obtained for all samples, except MORB8, recovered from 89 GPa (Table 2,

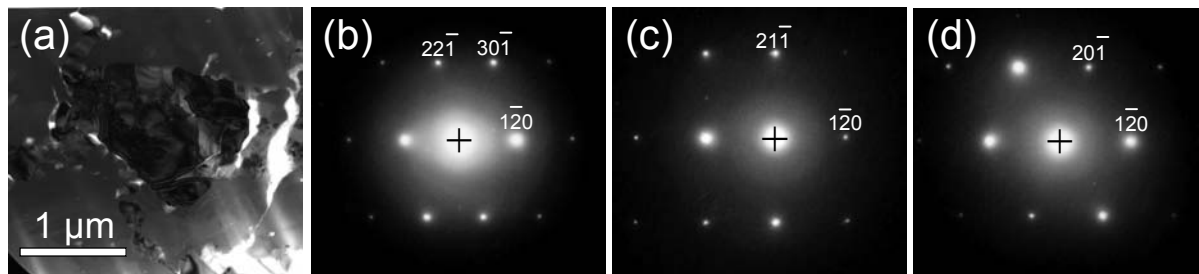
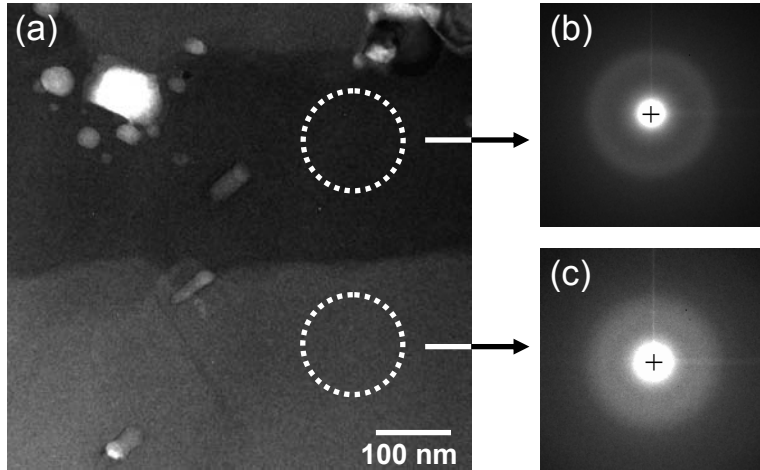
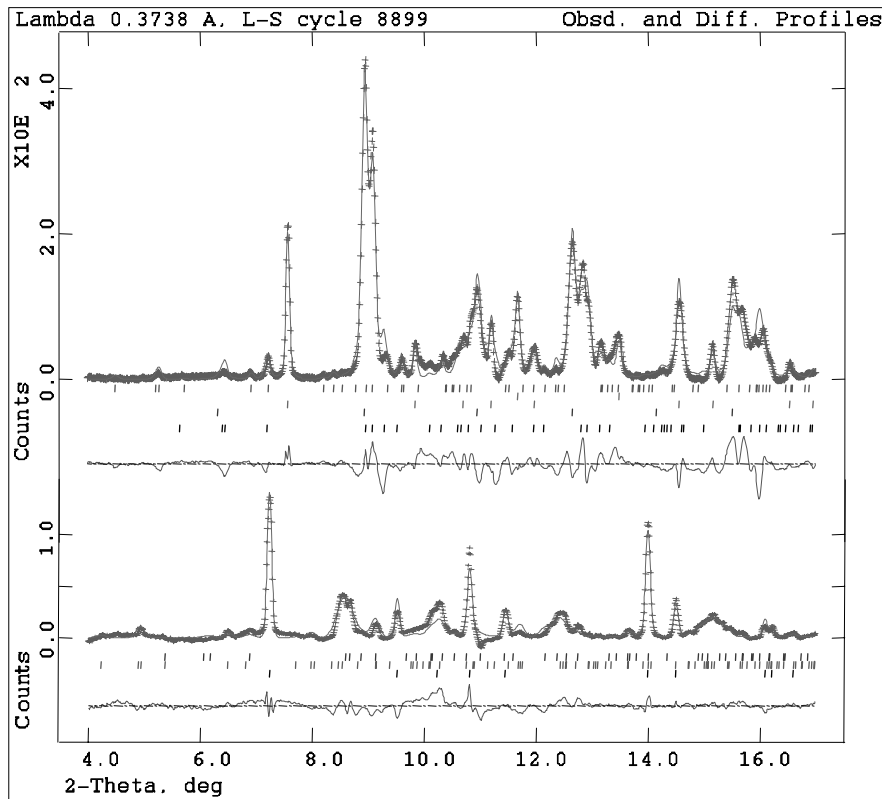


FIGURE 5. TEM bright-field micrograph of a stishovite particle with three SAED patterns indexed with stishovite structure  $P4_2/mnm$ . Zone axis  $[216]$ ,  $[215]$ ,  $[214]$  for (b), (c), and (d), respectively.



**FIGURE 6.** (a) The TEM image shows two easily distinguished gray amorphous zones: dark gray is enriched in Ca (Ca-perovskite) and light gray in Al, Mg, and Fe (Mg-perovskite). (b and c) Electron diffuse scattering patterns of amorphous Ca-perovskite and Mg-perovskite, respectively.



**FIGURE 7.** XRD patterns of a MORB sample at 43 GPa and 300 K (upper curve), and at ambient conditions (lower curve). Upper, high pressure, curve: tick marks indicate CF-type phase, neon (pressure-transmitting medium), stishovite, Ca-perovskite, and Mg-perovskite, from top to bottom. Lower, ambient, curve: tick marks indicate Mg-perovskite, CF-type phase, and stishovite, from top to bottom.

in atomic proportion). In this latter sample, the grain size was less than 100 nm, so it was impossible to obtain single phase compositions with FIB sections typically  $\sim 100$  nm in thickness. Table 1 compares our results with compositions measured on MORBs transformed at similar high-pressure and high-temperature conditions (Kesson et al. 1994; Hirose et al. 1999, 2005; Funamori et al. 2000; Miyajima et al. 2001; Ono et al. 2001). The modal mineralogy was estimated using mass-balance and by assuming that the bulk-

chemical composition of phases is equal to the starting composition (Table 1). Chemical mass balance showed that laser heated areas were affected by 20–40% iron loss and commensurate magnesium enrichment. Mg-Fe diffusion is moderate at the lowest pressures (less than 20%) and increases with pressure to about 40%. This effect could be linked to the width of the hot spot, which decreases with pressure (Kavner and Panero 2004). Iron loss is a feature typically observed in the laser-heated DAC samples due to the large

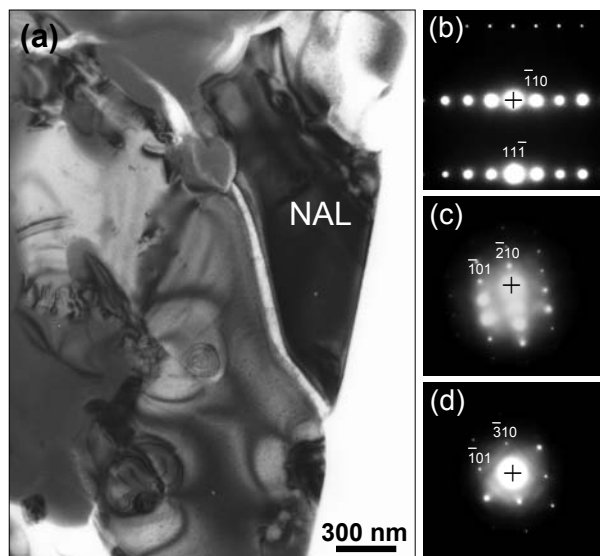


**FIGURE 8.** (a) TEM bright-field micrograph of the NAL phase at 33 GPa indexed with the structure  $P6_3/m$  proposed by Gasparick et al. (2000). Images b, c, and d are zone axis [112], [121], and [131], respectively.

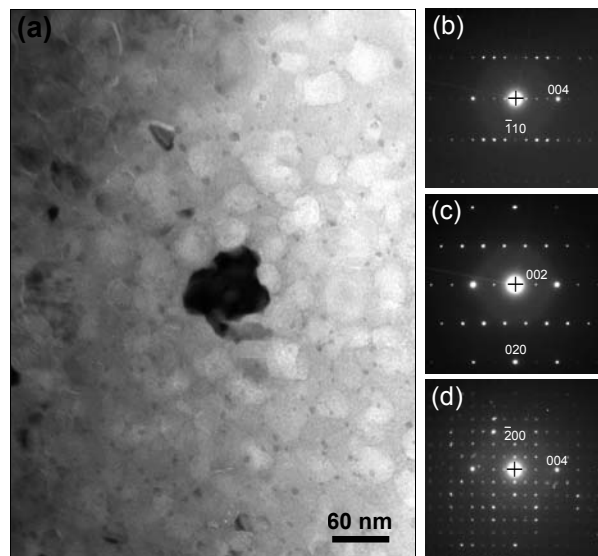


**FIGURE 9.** TEM bright-field micrograph of several nano-phases of calcium ferrite type structure in the sample recovered from 89 GPa and three SAED patterns indexed with the CF structure ( $Pbnm$ ) given by Yamada et al. (1983). Zone axis [110], [100], [010] for b, c, and d, respectively.

**TABLE 2.** Chemical composition of high-pressure phases in atomic proportion on the basis of 12 O atoms

Phase	Cation number (O = 12)							Cation sum
	Mg	Fe	Ca	Al	Si	Na	Ti	
<b>33 GPa</b>								
Mgpv	2.25 (25)	0.85 (6)	0.21 (11)	1.15 (5)	3.30 (11)	0.00 (0)	0.20 (0)	7.96 (14)
St	0.00 (0)	0.01 (1)	0.03 (2)	0.04 (1)	5.96 (2)	0.00 (1)	0.00 (0)	6.04 (2)
Capv	0.17 (12)	0.23 (9)	3.23 (21)	0.30 (3)	4.00	–	0.08 (2)	8.00
CF	1.45 (20)	0.89 (3)	0.11 (2)	3.39 (9)	1.98 (11)	1.17 (22)	0.02 (1)	9.00
NAL	1.98 (13)	0.54 (7)	0.17 (3)	3.44 (18)	1.99 (12)	0.86 (6)	0.02 (1)	9.00
<b>44 GPa</b>								
Mgpv	2.00 (13)	0.68 (9)	0.27 (6)	1.80 (11)	3.04 (9)	0.07 (4)	0.13 (2)	8.00 (8)
St	0.00 (1)	0.01 (1)	0.01 (1)	0.06 (1)	5.89 (11)	0.00 (0)	0.01 (1)	5.98 (11)
Capv	0.36 (17)	0.28 (6)	2.95 (17)	0.32 (7)	4.00	0.01 (1)	0.08 (1)	8.00
CF	1.24 (36)	0.61 (16)	0.11 (3)	3.53 (13)	2.14 (18)	1.35 (17)	0.03 (2)	9.00
NAL	2.07 (6)	0.29 (2)	0.15 (3)	3.91 (6)	1.71 (3)	0.85 (3)	0.02 (1)	9.00
<b>55 GPa</b>								
Mgpv	2.04 (7)	0.61 (3)	0.26 (2)	1.99 (7)	2.92 (4)	0.11 (2)	0.11 (1)	8.04 (3)
St	0.01 (1)	0.06 (1)	0.03 (2)	0.00 (0)	5.93 (1)	0.00 (0)	0.00 (0)	6.04 (1)
Capv	0.45 (12)	0.23 (4)	3.03 (22)	0.22 (6)	4.00	0.01 (1)	0.07 (0)	8.00
CF	1.42 (18)	0.38 (7)	0.14 (5)	3.77 (13)	1.98 (2)	1.30 (3)	0.01 (0)	9.00

Notes: Mgpv = Al-bearing magnesium perovskite; St = Stishovite; Capv = Calcium perovskite; CF = Calcium ferrite type phase; NAL = New aluminous phase.

thermal gradients (Hirose et al. 2005). We observed a concomitant Mg enrichment proportional to Fe loss. This enrichment also occurred in the study of Hirose et al. (2005). The main hosts of Fe and Mg are Mg-perovskite, CF-type phase, and NAL phase. Iron loss may introduce some error in the modal proportions of phases. If we assume that the partitioning of these elements between phases is not modified by the thermal diffusion in the heated spot (due to the Soret effect), it can be shown that correction of these elemental contents according to the mass-balance calculation leads, within error bars, to the same phase proportions.

The  $Al_2O_3$  content in the Mg-perovskite is 13 wt% in MORB1 and increases with pressure up to 24 wt% in MORB5 synthesized at 55 GPa. This result is in good agreement with the study of Hirose et al. (2001) on the system  $MgSiO_3$ - $Mg_3Al_2Si_3O_{12}$  where they observed the maximum solubility of  $Al_2O_3$  in perovskite

increasing with pressure from 1.4 mol% at 21 GPa to 13 mol% at 25 GPa. In addition, Walter et al. (2004, 2006) placed the solubility limit of  $Al_2O_3$  at about 25 mol% in an iron-free Al-bearing Mg-perovskite for pressures up to 83 GPa. Similarly, Miyajima et al. (1999) observed an orthorhombic Mg-perovskite structure with  $Al_2O_3$  contents up to 25 mol%.

The  $Al_2O_3$  content in CF-type phase increases with pressure, from 38 wt% at 33 GPa to 43 wt% once the NAL phase disappears at pressures exceeding 50 GPa. In addition, we note that the Al increase in CF-type phase and Mg-perovskite is mostly linked to the disappearance of the NAL phase. From 44 to 55 GPa, the proportion of Mg-perovskite also increased while the proportion of the aluminous phases decreased. These results indicate that the disappearance of the NAL phase is coupled with an increase in the proportion of Mg-perovskite that appears capable of hosting

a large amount of aluminum. This is consistent with the results of Miyajima et al. (1999), who observed the NAL phase at moderate pressure (30 GPa) but not at higher pressures in a pyrope garnet sample. The NAL disappearance could also be related to an increase in sodium solubility in the CF-type phase.

The CF-type and NAL phases are major hosts of aluminum and alkali elements in subducted MORBs since these phases may contain up to 37 wt%  $\text{Al}_2\text{O}_3$  and more than 5 wt%  $\text{Na}_2\text{O}$  (see Table 1). The CF-type phase contains more Na but less Al than the NAL phase. The NAL phase also contains a large amount of MgO, up to ~18 wt%. The CaO content in the NAL phase (2 wt%) is slightly higher than in the CF-type phase (1.3–1.7 wt%), as previously noticed by Guignot et al. (2004), whereas the FeO content is higher in the CF-type phase (10–14 wt%) than in the NAL phase (5–9 wt%). The Mg-perovskite hosts a larger amount of  $\text{TiO}_2$  than the Ca-perovskite, as observed by Ono et al. (2001). The  $\text{Al}_2\text{O}_3$  content of stishovite in our experiments was generally lower than 1 wt%, in contrast with the high  $\text{Al}_2\text{O}_3$  contents (>2 wt%) reported in the literature (Kesson et al. 1994; Funamori et al. 2000; Ono et al. 2001), but in agreement with the 1 wt%  $\text{Al}_2\text{O}_3$  measured by Hirose and Fei (2002) in stishovite synthesized from a basaltic composition. To check the Al content of our stishovite, EELS was performed on stishovite between 1400 and 1850 eV to measure the *L*-edge peak of Al and Si. After background subtraction, we calculated an Al/Si ratio of less than 0.01, corresponding to less than 1 wt%  $\text{Al}_2\text{O}_3$  in stishovite. The difference in Al content in stishovite between the different studies could be explained by the water content or by the synthesis temperature of the samples. Hydrogen incorporation in stishovite is obviously correlated with its Al content (e.g., Pawley et al. 1993; Ono 1999; Stebbins et al. 2006), H being easily incorporated in stishovite in the presence of Al. In addition, Panero et al. (2003) studied the transport of water into the mantle and observed an increase in the water content of stishovite during partial melting. They suggested that this behavior is related to the increasing Al content of stishovite above subsolidus temperatures. Finally, the difference in stishovite Al content between our study and Kesson et al. (1994) on the same starting composition could be ascribed to partial melting of the sample, as proposed by Panero et al. (2003), in agreement with the compositions of stishovite in MORB given in Litasov and Ohtani (2005) that shows in a similar manner an increasing Al content in stishovite close to the solidus.

## DISCUSSION

### High pressure-temperature MORB phases up to 44 GPa

The character and stability of phases in MORB as it subducts has important petrological and seismological implications, yet previous petrological studies in the multi-anvil at pressures up to 37 GPa have yielded conflicting results. Under these moderate-pressure conditions, there is widespread agreement that two perovskites and stishovite coexist, but the nature of the aluminous phase(s) is not agreed upon. Several studies have reported the presence of one Al-rich phase in basaltic compositions (Irfune and Ringwood 1993; Hirose et al. 1999; Funamori et al. 2000; Litasov and Ohtani 2005). Irfune and Ringwood (1993) observed an Al-rich phase at pressures around 25 GPa, for which they sug-

gested the CF-type structure. In addition, in their garnet transformation study at high pressures, Miyajima et al. (1999) synthesized an Al-bearing phase with hexagonal structure. By comparing XRD peaks with those reported by Irfune and Ringwood (1993), they suggested that it could be the NAL phase. Likewise, as reported in the recent study of Sanehira et al. (2006) on the NAL phase, Akaogi et al. (1999) obtained XRD peaks of the NAL phase similar to those of Irfune and Ringwood (1993), which they had attributed to the CF-type phase. Ono et al. (2001) also reported only the CF-type phase, but noted the presence of grains too small for microprobe investigation—possibly the NAL phase.

There have been previous reports of the coexistence of two Al-rich phases (CF and NAL) in natural MORB (Miyajima et al. 2001; Hirose and Fei 2002; Litasov et al. 2004). Miyajima et al. (2001) analyzed MORB containing 0.12 wt% of  $\text{K}_2\text{O}$  from a run at 27 GPa and 2473 K (Hirose et al. 1999), and reported both NAL and CF. We confirm the results of Miyajima et al. (2001): in the natural MORB samples investigated in this study, we observed five phases up to 44 GPa: Al-bearing Mg-perovskite, Ca-perovskite, stishovite, and two aluminous phases—the CF-type phase and the NAL phase. Our study confirms that two aluminous phases with distinct structures coexisting in MORBs at pressures up to 44 GPa, i.e., the hexagonal NAL phase and the CF-type phase.

### Stability of the NAL phase above 44 GPa

Ono et al. (2002b) observed the NAL structure up to 63 GPa and 1500 K using pure NAL as a starting composition. In contrast, our coupled observations using TEM (present study) and in situ XRD (Perrillat et al. 2006; Ricolleau, unpublished manuscript.) indicates that, for a MORB starting composition, the NAL phase disappears above 50 GPa. This finding highlights the importance of bulk composition on phase stability. In another example of the importance of composition, Akaogi et al. (1999) studied  $\text{MgAl}_2\text{O}_4$ - $\text{CaAl}_2\text{O}_4$  end-member solid solution and reported the presence of both aluminous phases with an increasing amount of the CF-type phase near the  $\text{CaAl}_2\text{O}_4$  end-member between pressures of 8 and 23 GPa.

On the other hand, we have shown that the CF-type phase is stable up to 85 GPa. We do not see any structural change of the  $\text{CaFe}_2\text{O}_4$  structure into the  $\text{CaTi}_2\text{O}_4$  structure (*Cmcm*) above 40 GPa as has been suggested by Funamori et al. (1998). Moreover, our composition is closer to the  $\text{NaAlSiO}_4$  end-member, for which such structural modification has not been observed (Guignot and Andrault 2004). Ono et al. (2005) observed this structural change only at pressures exceeding 130 GPa during in situ XRD, and similar observations were made by Hirose et al. (2005). It must be noted that very few chemical analysis are available for such samples. Hirose et al. (2005) were able to measure the chemical composition of quenched phases at 60 and 113 GPa for a MORB starting composition. Phases and compositions reported in their study are in good agreement with our own measurements at the same pressure, although some differences can be observed in the iron and aluminum contents (see Table 1 for details).

### Evolution of phase compositions with pressure and implications for subducting MORB

Our observation that the Al content of Mg-perovskite increases with increasing pressure is in good agreement with studies on

the post-garnet transformation whereby the corundum or NAL phase often coexists with Al-bearing Mg-perovskite (Irifune et al. 1996; Miyajima et al. 1999). Miyajima et al. (1999) also reported an increase in the Ca content of Mg-perovskite with pressure accompanied by a decrease of NAL phase abundance. It seems clear that the increase of Al and Na contents in Mg-perovskite and CF-type phase with increasing pressure is related to the disappearance of the NAL phase.

This compositional and mineralogical transformation takes place at lower mantle pressure and temperature conditions, between 1100 and 1250 km depth. Considering the small variability of chemical compositions reported among fresh or altered basalts, we assume this should not significantly modify phase relations reported in this study. We propose that such high-pressure mineralogical modifications could be related to some reported seismic heterogeneities. For example, many fast seismic anomalies associated with slab subduction are seen in the mid-mantle (e.g., Niu and Kawakatsu 1997; Vinnik et al. 2001; Kaneshima and Helffrich 2003; Niu et al. 2003). Niu and Kawakatsu (1997) detected large velocity increases under the Indonesia arc at depths of 940 to 1080 km from East to West. Likewise, Vinnik et al. (2001) observed discontinuities in several subduction environments at 1200 km depth with lateral variations in depth and amplitude. The cause of these anomalies is not well understood and is widely debated (Grand 2002; Castle and Van der Hilst 2003). The disappearance of the NAL phase and concomitant growth of Mg-perovskite at 50 GPa (corresponding to depths of ~1200 km) reported in this study may help to explain such lower mantle seismic anomalies. The variable depth of such discontinuities could be due to composition and temperature variations within the subducting slab. In our study, however, we have observed a gradual shift in the mineralogy with pressure and temperature, which is characteristic of a divariant transition. Therefore, our observations seem to be more compatible with an anomalous velocity increase in the mantle rather than a sharp discontinuity. A potential link between the observed seismic discontinuity and phase transformations, i.e., the orthorhombic-cubic transition in Al-bearing or pure Ca-perovskite (Kurashina et al. 2004; Adams and Oganov 2006, respectively) or the tetragonal-cubic transition (Shim et al. 2002; Ono et al. 2004) and the NAL phase disappearance, would benefit from detailed experimentation in the pressure range 40–50 GPa.

#### ACKNOWLEDGMENTS

We thank A. Gloter for his great help with the EELS measurements. We thank E. Cottrell and I. Savoy for useful comments on the paper as well as M. Walter and an anonymous reviewer for beneficial reviews. We thank J. Feinberg for editorial handling. This research was supported by CNRS INSU French program DyETI. EDX analysis were performed at the Laboratoire de Structure et Propriété de l'Etat Solide, on the TEM CM30 Philips, INSU National Instrument.

#### REFERENCES CITED

- Adams, D.J. and Oganov, A.R. (2006) Ab initio molecular dynamics study of CaSiO<sub>3</sub> perovskite at *P-T* conditions of Earth's lower mantle. *Physical Review B*, 73, 184106.
- Akaogi, M., Hamada, Y., Suzuki, T., Kobayashi, M., and Okada, M. (1999) High-pressure transitions in the system MgAl<sub>2</sub>O<sub>4</sub>-CaAl<sub>2</sub>O<sub>4</sub>: A new hexagonal aluminous phase with implication for the lower mantle. *Physics of the Earth and Planetary Interiors*, 115, 67–77.
- Andraut, D., Fiquet, G., Guyot, F., and Hanfland, M. (1998) Pressure-induced Landau-type transition in stishovite. *Science*, 282, 720–724.
- Andraut, D., Bolfan-Casanova, N., and Guignot, N. (2001) Equation of state of lower mantle (Al,Fe)-MgSiO<sub>3</sub> perovskite. *Earth and Planetary Science Letters*, 193, 501–508.
- Benzerara, K., Menguy, N., Guyot, F., Vanni, C., and Gillet, P. (2005) TEM study of a silicate-carbonate-microbe interface prepared by focused ion beam milling. *Geochimica et Cosmochimica Acta*, 69, 1413–1422.
- Carrez, P., Leroux, H., Cordier, P., and Guyot, F. (2001) Electron-irradiation-induced phase transformation and fractional volatilization in (Mg,Fe)<sub>2</sub>SiO<sub>4</sub> olivine thin films. *Philosophical Magazine A*, 81, 2823–2840.
- Castle, J.C. and van der Hilst, R. (2003) Searching for seismic scattering off mantle interfaces between 800 km and 2000 km depth. *Journal of Geophysical Research*, 108, 2095, DOI: 10.1029/2001JB000286.
- Chervin, J.C., Canny, B., Besson, J.M., and Pruzan, P. (1995) A diamond anvil cell for IR microspectroscopy. *Review of Scientific Instruments*, 66, 2595–2598.
- Cliff, G. and Lorimer, G.W. (1975) The quantitative analysis of thin specimens. *Journal de Microscopie*, 103, 203–207.
- Dubrovinsky, L.S., Dubrovinskaia, N.A., Prokopenko, V.B., and Le Bihan, T. (2002) Equation of state and crystal structure of NaAlSiO<sub>4</sub> with calcium-ferrite type structure in the conditions of the lower mantle. *High Pressure Research*, 22, 495–499.
- Funamori, N., Jeanloz, R., Nguyen, J.H., Kavner, A., Caldwell, W.A., Fujino, K., Miyajima, N., Shimmei, T., and Tomioka, N. (1998) High-pressure transformations in MgAl<sub>2</sub>O<sub>4</sub>. *Journal of Geophysical Research*, 103, 20813–20818.
- Funamori, N., Jeanloz, R., Miyajima, N., and Fujino, K. (2000) Mineral assemblages of basalt in the lower mantle. *Journal of Geophysical Research*, 105, 26037–26043.
- Gasparick, T., Tripathi, A., and Parise, J.B. (2000) Structure of a new Al-rich phase, (K, Na)<sub>0.8</sub>(Mg, Fe)<sub>2</sub>(Mg, Fe, Al, Si)<sub>6</sub>O<sub>12</sub>, synthesized. *American Mineralogist*, 85, 613–618.
- Giannuzzi, L.A. and Stevie, F.A. (1999) A review of focused ion beam milling techniques for TEM specimen preparation. *Micron*, 30, 197–204.
- Grand, S.P. (2002) Mantle shear-wave tomography and the fate of subducted slabs. *Philosophical Transactions of the Royal Society of London A*, 360, 2475–2491.
- Guignot, N. and Andraut, D. (2004) Equations of state of Na-K-Al host phases and implications for MORB density in the lower mantle. *Physics of the Earth and Planetary Interiors*, 143–144, 107–128.
- Heaney, P.J., Vicenzi, E.P., Giannuzzi, L.A., and Livi, K.J.T. (2001) Focused ion beam milling: A method of site-specific sample extraction for microanalysis of Earth and planetary materials. *American Mineralogist*, 86, 1094–1099.
- Hemley, R.J., Zha, C.S., and Jephcoat, A.P., Mao, H.K., Finger, L.W., and Cox, D.E. (1989) X-ray diffraction and equation of state of solid neon to 110 GPa. *Physical Review B*, 39, 1820–1827.
- Hirose, K. and Fei, Y. (2002) Subsolidus and melting-phase relations of basaltic composition in the uppermost lower mantle. *Geochimica et Cosmochimica Acta*, 66, 2099–2108.
- Hirose, K., Fei, Y., Ma, Y., and Mao, H.K. (1999) The fate of subducted basaltic crust in the Earth's lower mantle. *Nature*, 397, 53–56.
- Hirose, K., Fei, Y., Ono, S., Yagi, T., and Funakoshi, K. (2001) In situ measurements of the phase transition boundary in Mg<sub>3</sub>Al<sub>2</sub>Si<sub>3</sub>O<sub>12</sub>: Implications for the nature of the seismic discontinuities in the Earth's mantle. *Earth and Planetary Science Letters*, 184, 567–573.
- Hirose, K., Takafuji, N., Sata, N., and Ohishi, Y. (2005) Phase transition and density of subducted MORB crust in the lower mantle. *Earth and Planetary Science Letters*, 237, 239–251.
- Irifune, T. and Ringwood, A.E. (1993) Phase transformations in subducted oceanic crust and buoyancy relationships at depths of 600–800 km in the mantle. *Earth and Planetary Science Letters*, 117, 101–110.
- Irifune, T., Koizumi, T., and Ando, J. (1996) An experimental study of the garnet-perovskite transformation in the system MgSiO<sub>3</sub>-Mg<sub>3</sub>Al<sub>2</sub>Si<sub>3</sub>O<sub>12</sub>. *Physics of the Earth and Planetary Interiors*, 96, 147–157.
- Irifune, T., Isshiki, M., and Sakamoto, S. (2005) Transmission electron microscope observation of the high-pressure form of magnesite retrieved from laser heated diamond anvil cell. *Earth and Planetary Science Letters*, 239, 98–105.
- Kaneshima, S. and Helffrich, G. (2003) Subparallel dipping heterogeneities in the mid-lower mantle. *Journal of Geophysical Research*, 108, 2272, DOI: 10.1029/2001JB001596.
- Kavner, A. and Panero, W.R. (2004) Temperature gradients and evaluation of thermoelastic properties in the synchrotron-based laser-heated diamond cell. *Physics of the Earth and Planetary Interiors*, 143–144, 527–539.
- Kesson, S.E., Fitz Gerald, J.D., and Shelley, J.M.G. (1994) Mineral chemistry and density of subducted basaltic crust at lower-mantle pressures. *Nature*, 372, 767–769.
- Kurashina, T., Hirose, K., Ono, S., Sata, N., and Ohishi, Y. (2004) Phase transition in Al-bearing CaSiO<sub>3</sub> perovskite: Implications for seismic discontinuities in the lower mantle. *Physics of the Earth and Planetary Interiors*, 145, 67–74.
- Larson, A.C. and Von Dreele, R.B. (1994) General structure analysis system. Los Alamos Manual Report, 86, 748.
- Lee, K.K.M., O'Neill, B., and Jeanloz, R. (2004a) Limits to resolution in composition and density in ultra high-pressure experiments on natural mantle-rock

- samples. *Physics of the Earth and Planetary Interiors*, 143–144, 241–253.
- Lee, K.K.M., O'Neill, B., Panero, W.R., Shim, S., Benedetti, L.R., and Jeanloz, R. (2004b) Equations of state of the high-pressure phases of a natural peridotite and implications for the Earth's lower mantle. *Earth and Planetary Science Letters*, 223, 381–393.
- Litasov, K.D. and Ohtani, E. (2005) Phase relations in hydrous MORB at 18–28 GPa: Implications for heterogeneity of the lower mantle. *Physics of the Earth and Planetary Interiors*, 150, 239–263.
- Litasov, K., Ohtani, E., Suzuki, A., Kawazoe, T., and Funakoshi, K. (2004) Absence of density crossover between basalt and peridotite in the cold slabs passing through 660 km discontinuity. *Geophysical Research Letters*, 31, L24607.
- Liu, J., Zhang, J., Flesh, L., Li, B., Weidner, D.J., and Liebermann, R.C. (1999) Thermal equation of state of stishovite. *Physics of the Earth and Planetary Interiors*, 112, 257–266.
- Liu, L.G. (1977) High pressure NaAlSiO<sub>4</sub>: The first silicate calcium ferrite isotype. *Geophysical Research Letters*, 4, 183–186.
- Madon, M., Guyot, F., Peyronneau, J., and Poirier, J.P. (1989) Electron microscopy of high-pressure phases synthesized from natural olivine in diamond anvil cell. *Physics and Chemistry of Minerals*, 16, 320–330.
- Mao, H.K., Xu, J., and Bell, P.M. (1986) Calibration of the Ruby Gauge to 800 kbar Under Qasi-Hydrostatic Conditions. *Journal of Geophysical Research*, 91, 4673–4676.
- Miura, H., Hamada, Y., Suzuki, T., Akaogi, M., Miyajima, N., and Fujino, K. (2000) Crystal structure of CaMg<sub>2</sub>Al<sub>2</sub>O<sub>12</sub>, a new Al-rich high pressure form. *American Mineralogist*, 85, 1799–1803.
- Miyajima, N., Fujino, K., Funamori, N., Kondo, T., and Yagi, T. (1999) Garnet-perovskite transformation under conditions of Earth's lower mantle: an analytical transmission microscopy study. *Physics of the Earth and Planetary Interiors*, 116, 117–131.
- Miyajima, N., Yagi, T., Hirose, K., Kondo, T., Fujino, K., and Miura, H. (2001) Potential host phase of aluminum and potassium in the Earth's lower mantle. *American Mineralogist*, 86, 740–746.
- Murakami, M., Hirose, K., Sata, N., and Ohishi, Y. (2005) Post-perovskite phase transition and mineral chemistry in the pyrolytic lowermost mantle. *Geophysical Research Letters*, 32, L03304, DOI: 10.1029/2004GL021956.
- Niu, F. and Kawakatsu, H. (1997) Depth variation of the mid-mantle seismic discontinuity. *Geophysical Research Letters*, 24, 429–432.
- Niu, F., Kawakatsu, H., and Fukao, Y. (2003) Seismic evidence for a chemical heterogeneity in the midmantle: A strong and slightly dipping seismic reflector beneath the Mariana subduction zone. *Journal of Geophysical Research*, 108, 2419, DOI: 10.1029/2002JB002384.
- Oganov, A.R., Gillan, M.J., and Price, G.D. (2005) Structural stability of silica at high pressures and temperatures. *Physical Review B*, 71, 064104.
- Oguri, K., Funamori, N., Uchida, T., Miyajima, N., Yagi, T., and Fujino, K. (2000) Post-garnet transition in a natural pyrope: a multi-anvil study based on in situ X-ray diffraction and transmission electron microscopy. *Physics of the Earth and Planetary Interiors*, 122, 175–186.
- Ono, S. (1999) High temperature stability limit of phase egg, AlSiO<sub>3</sub>(OH). *Contributions to Mineralogy and Petrology*, 137, 83–89.
- Ono, S., Ito, E., and Katsura, T. (2001) Mineralogy of subducted basaltic crust (MORB) from 25 to 37 GPa, and chemical heterogeneity of the lower mantle. *Earth and Planetary Science Letters*, 190, 57–63.
- Ono, S., Hirose, K., Kikegawa, T., and Saito, Y. (2002a) The compressibility of a natural composition calcium ferrite-type aluminous phase to 70 GPa. *Physics of the Earth Planetary Interiors*, 131, 311–318.
- Ono, S., Hirose, K., Isshiki, M., Mibe, K., and Saito, Y. (2002b) Equation of state of hexagonal aluminous phase in basaltic composition to 63 GPa at 300 K. *Physics and Chemistry of Minerals*, 29, 527–531.
- Ono, S., Ohishi, Y., and Mibe, K. (2004) Phase transition of Ca-perovskite and stability of Al-bearing Mg-perovskite in the lower mantle. *American Mineralogist*, 89, 1480–1485.
- Ono, S., Ohishi, Y., Isshiki, M., and Watanuki, T. (2005) In situ X-ray observations of phase assemblages in peridotite and basalt compositions at lower mantle conditions: Implications for density of subducted oceanic plate. *Journal of Geophysical Research*, 110, B02208, DOI: 10.1029/2004JB003196.
- Panero, W.R., Benedetti, L.R., and Jeanloz, R. (2003) Transport of water into the lower mantle: Role of stishovite. *Journal of Geophysical Research*, 108, 2039, DOI: 10.1029/2002JB002053.
- Pawley, A.R., McMillan, P.F., and Holloway, J.R. (1993) Hydrogen in stishovite, with implications for mantle water-content. *Science*, 261, 1024–1026.
- Perrillat, J.P., Ricolleau, A., Daniel, I., Fiquet, G., Mezouar, M., Guignot, N., and Cardon, H. (2006) Phase transformations of subducted basaltic crust in the upmost lower mantle. *Physics of the Earth and Planetary Interiors*, 157, 139–149.
- Reusser, E., Kägi, R., Gasser, P., and Malmström, J. (2003) Focused ion beam technique as a preparation for chemical analysis at sub-micrometer scale. *Geophysical Research Abstract*, 5, 11579.
- Ricolleau, A., Fiquet, G., Perrillat, J.P., Daniel, I., Menguy, N., Cardon, H., Addad, A., and Vanni, C. (2004) The fate of subducted basaltic crust in the Earth's lower mantle: an experimental petrological study. *Eos Trans. AGU*, 85(47), Fall Meeting Supplement, Abstract U33B-02.
- Ringwood, A.E. and Major, A. (1971) Synthesis of majorite and other high pressure garnets and perovskites. *Earth and Planetary Science Letters*, 12, 411–418.
- Sanehira, T., Irifune, T., Shinmei, T., Brunet, F., Funakoshi, K., and Nozawa, A. (2006) In situ X-ray diffraction study of an aluminous phase in MORB under lower mantle conditions. *Physics and Chemistry of Minerals*, 33, 28–34.
- Schultz, E., Mezouar, M., Crichton, W., Bauchau, S., Blattmann, G., Andrault, D., Fiquet, G., Boehler, R., Rambert, N., Sitaud, B., and Loubeyre, P. (2005) Double-sided laser heating system for in situ high pressure- high temperature monochromatic X-ray diffraction at the ESRF. *High Pressure Research*, 25, 71–83.
- Shim, S.-H., Jeanloz, R., and Duffy, T.S. (2002) Tetragonal structure of CaSiO<sub>3</sub> perovskite above 20 GPa. *Geophysical Research Letters*, 29, 2166, DOI: 10.1029/2002GL016148.
- Shinmei, T., Sanehira, T., Yamazaki, D., Inoue, T., Irifune, T., Funakoshi, K., and Nozawa, A. (2005) High-temperature and high-pressure equation of state for the hexagonal phase in the system NaAlSiO<sub>4</sub>-MgAl<sub>2</sub>O<sub>4</sub>. *Physics and Chemistry of Minerals*, 32, 594–602.
- Stebbins, J.F., Du, L.S., Kelsey, K., Kojitani, H., Akaogi, M., and Ono, S. (2006) Aluminum substitution in stishovite and MgSiO<sub>3</sub> perovskite: High-resolution <sup>27</sup>Al NMR. *American Mineralogist*, 91, 337–343.
- Tutti, F., Dubrovinsky, L.S., and Saxena, S.K. (2000) High pressure transformation of jadeite and stability of NaAlSiO<sub>4</sub> with Calcium-ferrite type structure in the lower mantle conditions. *Geophysical Research Letters*, 27, 2025–2028.
- Van Cappellen, E. (1990) The parameterless correction method in X-ray microanalysis. *Microscopy Microanalysis and Microstructure*, 1, 1–22.
- Van Cappellen, E. and Doukhan, J.C. (1994) Quantitative transmission X-ray microanalysis of ionic compounds. *Ultramicroscopy*, 53, 343–349.
- Vanpeteghem, C.B., Ohtani, E., Litasov, K., Kondo, T., Watanuki, T., Isshiki, M., and Takemura, K. (2003) The compressibility of hexagonal Al-rich NAL phase: similarities and differences with calcium ferrite-type (CF) phase with implications for the lower mantle. *Physics of the Earth Planetary Interiors*, 138, 223–230.
- Vinnik, L., Kato, M., and Kawakatsu, H. (2001) Search for seismic discontinuities in the lower mantle. *Geophysical Journal International*, 147, 41–56.
- Walter, M.J., Kubo, A., Yoshino, T., Brodholt, J., Koga, K.T., and Ohishi, Y. (2004) Phase relations and equation-of-state of aluminous Mg-silicate perovskite and implications for Earth's lower mantle. *Earth and Planetary Science Letters*, 222, 501–516.
- Walter, M.J., Tronnes, R.G., Armstrong, L.S., Lord, O.T., Caldwell, W.A., and Clark, S.M. (2006) Subsolidus phase relations and perovskite compressibility in the system MgO-Al<sub>2</sub>O<sub>3</sub>-SiO<sub>2</sub> with implications for Earth's lower mantle. *Earth and Planetary Science Letters*, 248, 77–89.
- Yagi, T., Okabe, K., Nishiyama, N., Kubo, A., and Kikegawa, T. (2004) Complicated effects of aluminum on the compressibility of silicate perovskite. *Physics of the Earth and Planetary Interiors*, 143–144, 81–91.
- Yamada, H., Matsui, Y., and Ito, E. (1983) Crystal-chemical characterization of NaAlSiO<sub>4</sub> with the CaFe<sub>2</sub>O<sub>4</sub> structure. *Mineralogical Magazine*, 47, 177–181.
- Yutani, M., Yagi, T., Yusa, H., and Irifune, T. (1997) Compressibility of calcium ferrite-type MgAl<sub>2</sub>O<sub>4</sub>. *Physics and Chemistry of Minerals*, 24, 340–344.

MANUSCRIPT RECEIVED DECEMBER 5, 2006

MANUSCRIPT ACCEPTED SEPTEMBER 10, 2007

MANUSCRIPT HANDLED BY JOSHUA FEINBERG